

## ARTICLE

## Direct Numerical Simulation of MHD Turbulent Flows with High-Pr Heat Transfer

Yoshinobu YAMAMOTO\* and Tomoaki KUNUGI

Kyoto University, Yoshida, Sakyo, Kyoto, 606-8501, Japan

The large-scale direct numerical simulations (DNS) of a Magneto-Hydro-Dynamics (MHD) turbulent heat transfer have been executed on massively parallel processing supercomputer systems. The maximum computational speed was measured up 5.28 Tflops and the sufficiently parallelization efficiency by using up to over thousands CPUs was achieved. The DNS results were in good agreements with the previous experimental data and we proposed new MHD heat transfer equation:  $Nu/Nu_{Ha=0} = 1-5.5 N$ , where  $Nu$  is the Nusselt number,  $Ha$  is the Hartman number and  $N$  is the interaction parameter. Definitely, we can succeed to establish the DNS data of MHD heat transfer under the high-Re (= 14,000) and the wide-range Prandtl number conditions ( $Pr = 0.025-25$ ).

**KEYWORDS:** MHD, high-Pr, high-Re, DNS, parallel computing

## I. Introduction

FLiBe which is the molten salt mixture of LiF and BeF is one of the coolant candidates in a first wall and blanket of the fusion reactors, and has several advantages which are little Magneto-Hydro-Dynamics (MHD) pressure loss, good chemical stability, less solubility of tritium and so on. In contrast, low thermal diffusivity and high viscosity are the key issues of the FLiBe utilization as a coolant.<sup>1)</sup> Moreover, developments of MHD turbulence model with high accuracy are highly demanded to predict the MHD pressure loss and the heat transfer for fusion reactor designs.

MHD turbulent wall-bounded flows have been investigated extensively by both experimental and numerical studies (Reed and Lykoudis,<sup>2)</sup> Simomura,<sup>3)</sup> Noguchi *et al.*,<sup>4)</sup> Orlandi,<sup>5)</sup> Satake *et al.*,<sup>6)</sup> Lee and Choi<sup>7)</sup> etc.) and many important information about drag reduction and turbulent modulation have been obtained. Especially, a direct numerical simulation (DNS) of turbulent flows is one of the most powerful methods to understand turbulent structures and heat transfer. Molten salt fluids such as FLiBe are the higher Pr fluids ( $Pr = \nu/\alpha$ : Prandtl number = 20-40,  $\nu$  is the kinetic viscosity,  $\alpha$  is the thermal diffusivity), however the previous DNS studies have conducted at the only lower Pr condition. Therefore, MHD turbulent heat transfer on higher Pr fluids hasn't been understood well. Furthermore, a problem of DNS studies limited to lower-Re ( $= U_b 2h/\nu$  is the bulk Reynolds number,  $U_b$  is the bulk mean velocity,  $h$  is the channel height) and -Pr conditions would be depended on the computational resources limitation.

In this study, DNS of MHD heat transfer under the high-Re (= 14,000) and the wide-range Pr conditions ( $Pr = 0.025-25$ ) have been executed on the massively parallel processing supercomputer systems. Present DNS achieved that the maximum grid number was  $O(10^9)$  and the maxi-

imum computational speed was measured up 5.28 Tflops. Eventually, detailed DNS database of MHD heat transfer in the high-Re and -Pr range were established.

## II. Numerical Methods

## 1. Basic Equations and Boundary Condition

The target flow is an incompressible MHD turbulent flows at a low magnetic Reynolds number ( $Re_m = U_b 2h/\eta$ ,  $\eta$  is the magnetic diffusivity) with passive scalar transport. The objective flow geometry and coordinate system are shown in Fig. 1.

Basic equations of the present DNS were the continuity equation (1), the momentum equations (2) with the electric field described using the electrical potential approach,<sup>3)</sup> Poisson equation (3) of the electrical potential, and the energy equation (4), respectively.

$$\frac{\partial u_i^*}{\partial x_i} = 0, \quad (1)$$

$$\frac{\partial u_i^*}{\partial t} + \frac{\partial u_i^* u_j^*}{\partial x_j} = F \delta_{i1} - \frac{\partial}{\partial x_i} \left( \frac{p^*}{\rho} \right) + \nu \frac{\partial^2 u_i^*}{\partial x_j \partial x_j} + \frac{\sigma}{\rho} \varepsilon_{ijk} \left( -\frac{\partial \phi^*}{\partial x_j} + \varepsilon_{jlm} u_l^* B_m \right) B_k, \quad (2)$$

$$\frac{\partial^2 \phi^*}{\partial x_i \partial x_i} = \frac{\partial}{\partial x_i} \left( \varepsilon_{ijk} u_j^* B_k \right), \quad (3)$$

$$\frac{\partial \theta^*}{\partial t} + \frac{\partial \theta^* u_j^*}{\partial x_j} = \alpha \frac{\partial^2 \theta^*}{\partial x_j \partial x_j}. \quad (4)$$

Here  $u_i (= u, v, w (i = 1, 2, 3))$  is the streamwise velocity ( $i = 1$ ), the vertical velocity ( $i = 2$ ) and the spanwise velocity ( $i = 3$ ),  $t$  is time,  $x_i (= x, y, z (i = 1, 2, 3))$  is the streamwise direction ( $i = 1$ ), the vertical direction ( $i = 2$ ) and the spanwise direction ( $i = 3$ ),  $F$  is the streamwise external force,  $p$  is the pressure,  $\rho$  is the density,  $\sigma$  is the

\*Corresponding author, E-mail: yyama@nucleng.kyoto-u.ac.jp

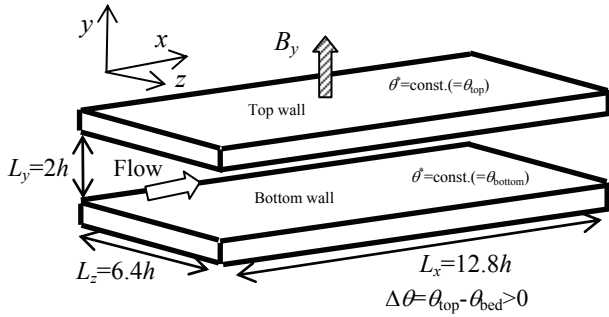


Fig. 1 Flow geometry and coordinate system

electrical conductivity,  $\phi$  is the electric potential,  $B_i = (0, B_y, 0)$  is the Magnetic flux density, and  $\theta$  is the temperature. Super script \* denotes instantaneous value and  $\delta_{ij}$ ,  $\epsilon_{ijk}$  ( $i, j, k = 1-3$ ) is the Kronecker delta and the Levi-Civita symbol, respectively.

Non-slip and periodic conditions were imposed for boundary conditions of velocity and the constant temperature at top and bottom boundaries ( $\theta_{top} > \theta_{bed}$ ,  $\theta_{top}$ : top wall temperature,  $\theta_{bed}$ : Bottom wall temperature), and the periodic conditions were imposed for a passive scalar field. Total electric current in the flow domain was kept zero and the boundary condition of the electric potential was non-conducting condition at all walls and the periodic condition imposed on the horizontal directions.

2. Numerical Procedures

The spectral method is used to compute the spatial discretization in the stream ( $x$ ) and spanwise ( $z$ ) directions. Nonlinear terms were computed with 1.5 times finer grids in horizontal ( $x$  and  $z$ ) directions to remove the aliasing errors (Padding method). The derivative in the wall normal ( $y$ ) direction is computed by a second-order finite difference scheme at the staggered grid arrangement. Time integration method is 3rd-order Runge-Kutta scheme for the convection terms, Crank-Nicolson scheme for the viscous terms and Euler Implicit scheme for the Pressure terms, respectively. The Helmholtz equation for the viscous (diffusion) terms and the Poisson equations of the pressure and the electrical potential are solved by a TriDiagonal Matrix Algorithm, TDMA in Fourier space.

3. Parallelization

In this DNS study, the Message Passing Interface (MPI) was adapted for a distributed memory parallel programming tool. Domain decomposition in the  $y$  direction was used in order to calculate 2D-FFTs for the horizontal directions ( $x, y$ ). Before performing the TDMA along the  $y$  direction, we need to transpose the data from the domain decomposition along the  $y$  axis to the one along the  $z$  axis as shown in Figs. 2(a) and (b). In this process, we implemented the following three methods to treat the discontinuous data transfer.

- 1) Data transposition by MPI\_ISEND/IRECIVE with the derivative data type discontinuous data.
- 2) Data transposition by MPI\_ISEND/IRECIVE with the packed 1D continuous data.

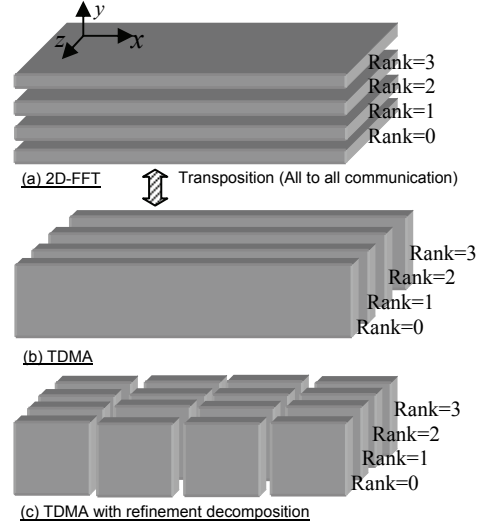


Fig. 2 1-D domain decomposition and transposition between 2D-FFTs and TDMA algorithms in case of 4 PEs

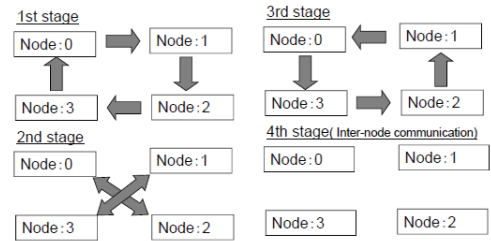


Fig. 3 Scheduling the multi-stages inter-node data communications in case of 4 nodes

- 3) Data transposition by remote memory access (RMA), called one-sided communication with the packed 1D continuous data.

Since the global memory function<sup>9)</sup> for the data transfer by the MPI library was implemented in the Earth Simulator (ES)<sup>10)</sup> and SX-9,<sup>11)</sup> faster data transfer by used MPI\_PUT based on RMA, called one-sided communication, can be expected in the ES and SX-9.

To avoid the excessively concentration of the data communication between the specified rank and others, scheduling<sup>12)</sup> the multi-stages internode data communications via the single-stage crossbar network, were implemented as shown in Fig. 3.

To reduce the data communication traffics, a hybrid parallelization by MPI and Microtasking was implemented.

Furthermore, to obtain the sufficient parallelization efficiency by using up to thousands CPUs in case of the ES, the phase shift method, in which a convolutional sum is obtained for a shifted grid system as well as for the original grid system, was adapted instead by the padding method. Using the phase shift method, we can reduce the load of memory copy in the padding method.

On the other hands, the special function such as the global memory function was not implemented on the T2K Open

**Table 1** Numerical condition

	Computer	$Re_\tau$	Ha	Pr	Domain $L_x, L_y, L_z$	Grid number $N_x, N_y, N_z$	Resolution $\Delta x^+, \Delta y^+, \Delta z^+$	Time integration length, $t^+$
CASE1 (Li)	T2K	400	0,20,28	0.025	12.8h, 2h, 6.4h	288, 432, 288	17.8,0.25-2.0,8.9	3,000-15,000
CASE2 (KOH)	T2K		0,16,20, 24,28,32	5.25				
CASE3 (FLiBe)	SX-9/ES		0,20 28	25.0		2048,870,1024	2.5,0.05-1.0,2.5	

Supercomputer<sup>13)</sup> and the overlapping of communication with computation algorithm was implemented. This means that data transposition from the domain decomposition along the  $y$  axis to the one along both of the  $x$  and  $z$  axis as shown in Fig. 2(a) and (c) and the communication, which is to transpose data by using MPI\_ISEND/IRECIVE with the packed 1D continuous data, was overlapped with the computation of TDMA.

#### 4. Numerical Condition

Numerical conditions of DNS for 2-D fully-developed turbulent channel flows imposed wall-normal magnetic field, were tabled in **Table 1**, where super-script + denotes the nondimensional quantities normalized by the friction velocity and the kinematic viscosity. In the computations, three thermal properties of the Lithium ( $Pr = \nu/\alpha$ :Prandtl number = 0.025), KOH solution ( $Pr = 5.25$ ), and FLiBe ( $Pr = 25$ ) were used. Note that the KOH solution was used as the FLiBe simulant fluid in the previous experimental study<sup>14)</sup> and Heat transfer data was obtained in case of KOH solution.

Turbulent Reynolds number ( $Re_\tau = u_\tau h/\nu$ ) was kept constant, 400, and Hartman number ( $Ha = B_y 2h(\sigma/\rho\nu)^{1/2}$ ) was changed from 0 to 28. Present numerical conditions of  $Re_\tau$  and  $Ha$  were almost in the same range of the experimental conditions.<sup>14)</sup>

CASE1 and 2 were calculated by using the T2K Open Supercomputer and CASE3 was calculated by using the SX-9 and ES.

### III. Performance of Parallel Computation

#### 1. T2K Open Supercomputer

We have measured the elapsed time for 100 time steps in CASE 1 by using the MPI function MPI\_wtime. Elapsed time per one time step was about 4.5 [s] when using 2nodes (16cores). The corresponding numbers of nodes (cores) taken up in the T2K were 1(16), 2(32), 3(48), and 6(96). Performance of the parallelization method 2) with overlapped communication algorithm exceeded only when using 6 nodes, compared with the parallelization method 1). The best number of the decomposition for  $z$  direction was 8. These implied that the overhead of the refinement decomposition and the overlapped process cannot be ignored when using small number of CPUs and the optimization of the decomposition number for  $z$  direction might be required under other calculation conditions.

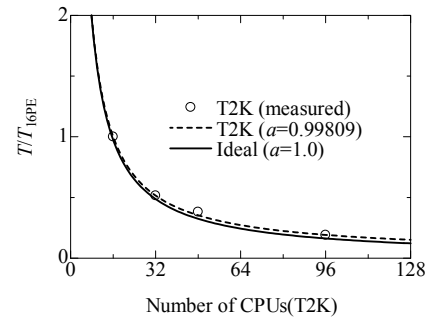


**Fig. 4** Elapsed time as a function of number of CPUs in T2K Open Supercomputer

**Figure 4** shows the elapsed time normalized by one when using 1 node (16 cores), where 6 nodes case was results by method 3) with overlapped communication algorithm and others were them by method 1). Parallel efficiency when using 6 nodes (96 cores) was 84.6% and parallelization rate ( $a$ ) was 0.99809.

#### 2. SX-9 and Earth Simulator

Using the program information of MPI/SX,<sup>9)</sup> computational speed in CASE3 has been measured for the calculation of 10 time steps and 100 time steps in the SX-9 and the ES, respectively. This computational speed taken in initialization was included from the measurement. The corresponding numbers of nodes (CPUs) taken up in the SX-9 were 4(64), 8(128) and 16(256) and 4 microtasking process per node were adapted in all cases. The numbers of nodes taken up in the ES were 256(1792) and 256(2,048), and 7 and 8 microtasking processes per node were adapted, respectively.

Using the padding method, parallelization method 3) with the scheduling inter-node communication was applied in case of the SX-9, because the performance loss in the parallelization method 1) was sensible when using 4 nodes (64 CPUs).

Parallelization method 1) with padding method (or phase shift method) was applied in case of the ES.

**Figure 5** shows the computational speed [Tflops] as a function of numbers of CPUs in the SX-9 and ES.

Computational speed was 4.21 Tflops, parallel efficiency was 74.3%, parallelization rate was 0.99865, and vector operation ratio was 99.71%, when using 16 nodes (256 CPUs) of the SX-9.

Computational speed in case of the phase shift method was 5.28 Tflops, parallel efficiency was 63.2%, paralleliza-

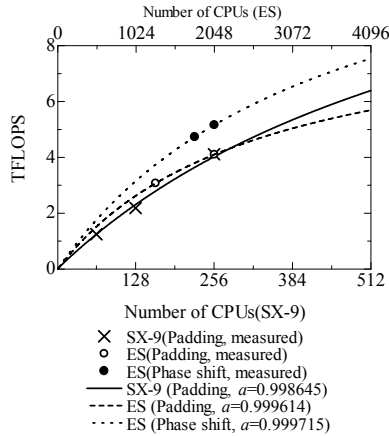


**Fig. 5** Computational speed [Tflops] as a function of number of CPUs in SX-9 and ES

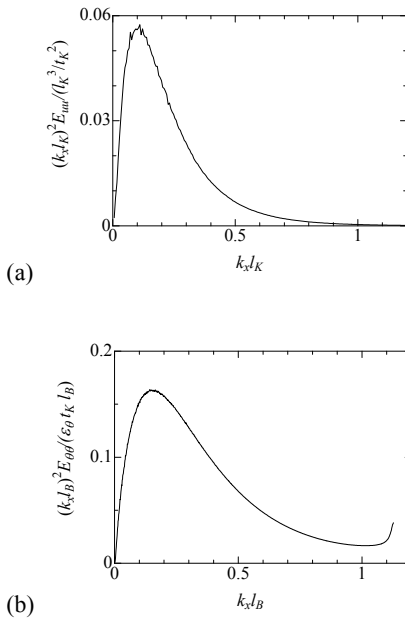
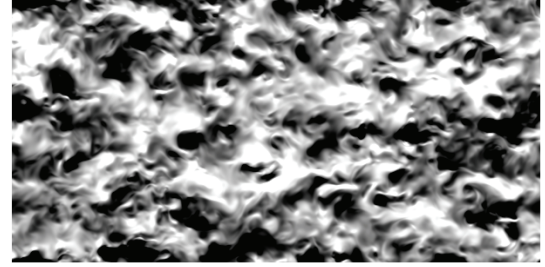


**Fig. 6** 1D-streamwise pre-multiplied energy spectra near channel center in CASE3,  $Ha = 0$ , 1) streamwise velocity and 2) temperature

tion rate was 0.99972, and vector operation ratio was 99.11%, when using 256 nodes (2,048 CPUs) of the ES. The phase shift method was 25% faster than the padding method in case of the ES. In case of the padding method, computational speed when using 256 nodes (2,048 CPUs) of the ES and 16 nodes (256 CPUs) of the SX-9 were almost same speed. Therefore, the performance loss in the parallelization method 1) observed in the SX-9, might be small in case of the ES.

Elapsed time per one time step was about 3.1 [s] when using 4 nodes (64 CPUs) in case of the SX-9.



(a)



(b)

**Fig. 7** Visualization in CASE3,  $Ha=0$ , near channel center, top view, 1) streamwise turbulent velocity,  $-0.1(\text{black}) < u^+ < 0.1(\text{white})$ , 2) turbulent temperature,  $-0.04(\text{black}) < \theta/(\Delta\theta:(\theta_{\text{top}}-\theta_{\text{bed}})) < 0.04(\text{white})$

## IV. DNS Results

### 1. Validation of Grid Resolution

**Figures 6(a)** and **(b)** show one-dimensional streamwise pre-multiplied energy spectra of streamwise velocity and temperature near channel center in CASE3, where  $k_x$  is the streamwise wave number and energy spectra were normalized by Kolmogorov scale ( $l_K$ ) and energy dissipation rate ( $\epsilon$ ) and Batchelor scale ( $l_B$ ) and temperature energy dissipation rate ( $\epsilon_0$ ), respectively. In the high-accuracy DNS, it was pointed out<sup>15</sup> that more than  $1 k_x l_K$  and  $k_x l_B$  of grid resolution were required for velocity and temperature field, respectively. In this DNS, it can be confirmed that more than  $1 k_x l_K$  and  $k_x l_B$  of grid resolution were resolved for velocity and temperature field, respectively.

### 2. Visualization

**Figures 7(a)** and **(b)** show the instantaneous streamwise turbulent velocity and turbulent temperature in CASE3,  $Ha = 0$ , respectively. In the high-Pr temperature field, fine small turbulent fluctuations were observed compared with the velocity field.

**Figures 8(a) - (f)** show the instantaneous turbulent velocities and temperature in CASE2. Compared between non-MHD field as shown in **Figs. 8(a)** and **(b)** and MHD field of them as shown in **Figs. 8(d)** and **(e)**, it can be understood that turbulent fluctuations were dramatically restricted channel center area, due to the MHD effects. However, larger-scale turbulent structures of the MHD temperature field as shown in **Fig. 8(f)** than them of non-MHD temperature field as shown in **Fig. 8(c)**, were existed. This might be affected by the high- Re and -Pr effects.

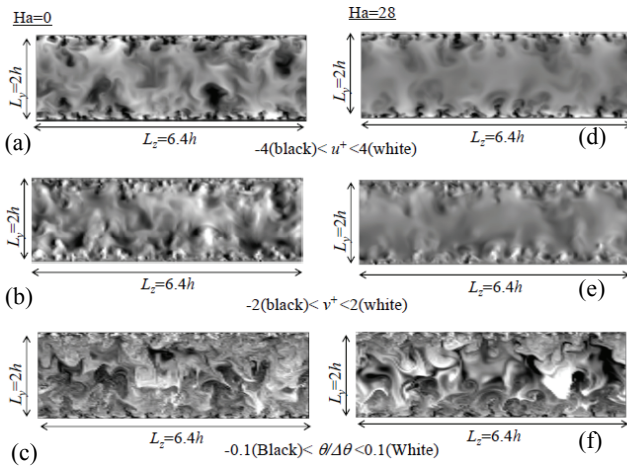


**Fig. 8** Visualization in CASE2, end view, (a) streamwise turbulent velocity,  $Ha = 0$ , (b) vertical turbulent velocity,  $Ha = 0$ , and (c) turbulent temperature,  $Ha = 0$ , (d), (e), and (f) is same as (1), 2), and 3) but  $Ha = 28$ , respectively.

### 3. MHD Heat Transfer

**Figure 9** shows the decrease in Nusselt number ( $Nu$ ) as a function of interaction parameter ( $N = Ha^2/Re$ ). The longitudinal axis is the ratio of Nusselt number normalized by Nusselt number of non-MHD case. Experimental results by Yokomine *et al.*<sup>14)</sup> and the correlation proposed by Blum<sup>16)</sup> is also plotted. Present DNS results of CASE2,  $Pr = 5.25$ , were in good agreements with experimental results.<sup>13)</sup> Furthermore, results in CASE3,  $Pr = 25$ , were also corresponded to them of CASE2 and experimental study.<sup>14)</sup> This indicates that similarity might be existed between medium high- $Pr(= 5.25)$  case and the high- $Pr(= 25)$  case. Therefore, we will propose the following correlation equation (5) in the high- $Pr$  range ( $Pr > 2$ ),

$$Nu/Nu_{Ha=0} = 1 - 5.5 Ha^2/Re. \quad (5)$$

On the other hands, DNS results of CASE1,  $Pr = 0.025$  were fitted in the correlation by Blum.<sup>16)</sup> The correlation proposed by Blum might be effective in the low- $Pr$  range ( $Pr \ll 1$ ).

### V. Conclusion

Using the high performance computing techniques, DNSs of MHD heat transfer in the high- $Re$  and the wide-range  $Pr$  have been executed on the supercomputer systems. It has been confirmed that present DNSs have the sufficient spatial resolution in the higher- $Pr(= 25)$  case.

Due to the MHD effects, turbulent fluctuations were dramatically restricted channel center area, but the large-scale turbulent structures of the temperature field were observed far from the wall region.

Present DNS results of the high- $Pr$  heat transfer were in good agreements with experimental results.<sup>14)</sup> It was suggested that the similarity might be existed between the medium high- $Pr(= 5.25)$  case and the high- $Pr(= 25)$  case. In the high- $Pr$  range ( $Pr > 2$ ), new correlation equation was proposed based on the present DNS data.

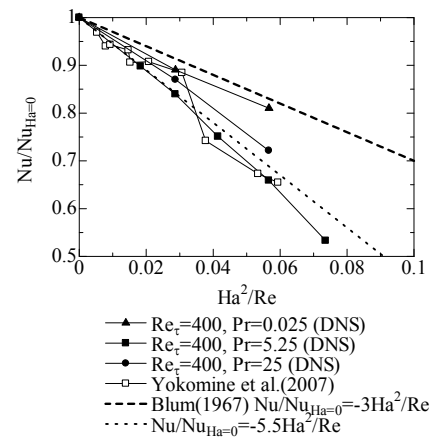


**Fig. 9** Degradation of heat transfer as a function interaction parameter ( $N = Ha^2/Re$ )

On the other hands, the correlation equation proposed by Blum<sup>16)</sup> might be effective in the low- $Pr$  ( $\ll 1$ ) range.

### Acknowledgment

Present DNSs were conducted by using the SX-9 supercomputer system at the Cyber Science Center, Tohoku University and the T2K open supercomputer at ACCMS and IIMC, Kyoto University. This study was supported by the Global COE program “Energy Science in the Age of Global Warming” and a Grant-in-aid for Young Scientists (B), KAKENHI (21760156) MEXT, Japan.

### References

- 1) A. Sagara, O. Motojima, K. Watanabe, S. Imagawa, H. Yamanishi, O. Mitarai, T. Sato, H. Chikaraishi, FFHR Group, “Blanket and Divertor Design for Force Free Helical Reactor (FFHR),” *Fusion Eng. Des.*, **29**, 51 (1995).
- 2) C. B. Reed, P. S. Lykoudis, “The effects of a transverse magnetic field on shear turbulence,” *J. Fluid Mech.*, **89**, 144 (1978).
- 3) Y. Simomura, “Large eddy simulation of magneto-hydrodynamic turbulent channel flows under a uniform magnetic field,” *Phys. Fluids*, **A3**, 3098 (1991).
- 4) P. Orlandi, “Drag reduction in turbulent MHD pipe flows,” *CTR, Proceedings of the Summer Program*, 447 (1996).
- 5) H. Noguchi, Y. Ohtsubo, N. Kasagi, [ftp.thtlab.t.u-tokyo.ac.jp/DNS](http://ftp.thtlab.t.u-tokyo.ac.jp/DNS) (1998).
- 6) S. Satale, T. Kunugi, K. Takase, Y. Ose, “Direct numerical simulation of turbulent flow under a uniform magnetic field for large-scale structures at high Reynolds number,” *Phys. Fluids*, **18**, 125106 (2006).
- 7) D. Lee, H. Choi, “Magneto-hydrodynamic turbulent flow in a channel at low magnetic Reynolds number,” *J. Fluid Mech.*, **439**, 367 (2001).
- 8) T. Boeck, D. Krasnov, E. Zienicke, “Numerical study of turbulent magneto-hydrodynamic channel flow,” *J. Fluid Mech.*, **572**, 179 (2007).
- 9) NEC Corporation, “SUPER-UX - MPI/SX RIYO NO TEBIKI (SUPER-UX -MPI/SX Operation Guide),” (2008).
- 10) Earth Simulator, <http://www.jamstec.go.jp/es/en/index.html>.
- 11) SX-9 supercomputer at Tohoku University’s Cyber Science Center, <http://www.isc.tohoku.ac.jp/HTML/>

- 12) H. Kobayashi *et al.*, "Performance evaluation of the SX-7 supercomputer on HPCC," [http://www.ss.isc.tohoku.ac.jp/refer/senac.html#2006\\_1](http://www.ss.isc.tohoku.ac.jp/refer/senac.html#2006_1) (2006), [in Japanese].
  - 13) T2K Open Supercomputer, <http://web.kudpc.kyoto-u.ac.jp/hpc/en/supercomputer>
  - 14) T. Yokomine, J. Takeuchi, H. Nakaharai, S. Satake, T. Kunugi, N. B. Morley, M. A. Abdou, "Experimental investigation of turbulent heat transfer of high Prandtl number fluid flow under strong magnetic field," *Fusion Sci. Tech.*, **52**, 625-629 (2007).
  - 15) V. Eswaran, S. B. Pope, "An examination of forcing in direct numerical simulations of turbulence," *Comput Fluid*, **16**, 258-278 (1988).
  - 16) E. Ya. Blume, "Effect of a magnetic field on heat transfer in the turbulent flow of conducting liquid," *High Temp.*, **5**, 68-74 (1967).
-